ANL/ET/CP--90230
CONF-960106--13

Sanjay Ahuja[1], William A. Ellingson[1], J. Scott Steckenrider,[2] and Steven Koch[3]

INFRARED-BASED NDE METHODS FOR DETERMINING THERMAL PROPERTIES AND DEFECTS IN CERAMIC COMPOSITES*.

REFERENCE: Ahuja, S., Ellingson, W. A., Steckenrider, J. S., and Koch, S., "Infrared-Based NDE Methods for Determining Thermal Properties and Defects in Ceramics", Thermal and Mechanical Test Methods and Behavior of Continuous-Fiber Ceramic Composites, ASTM STP 1309, Michael G. Jenkins, Stephen T. Gonczy, Edgar Lara-Curzio, Noel E. Ashbaugh, and Larry P. Zawada, Eds., American Society for Testing and Materials, Philadelphia, 1996.

ABSTRACT: Continuous-fiber ceramic matrix composites are currently being developed for various high temperature applications, including use in advanced heat engines. In the material classes of interest for such applications, i.e., silicon carbide (SiC)-fiber-reinforced SiC ($SiC_{(f)}/SiC$), SiC-fiber-reinforced silicon nitride ($SiC_{(f)}/Si_3N_4$), $Al_2O_{3(f)}/Al_2O_3$, etc., the condition of the interface between the fibers and matrix is critical to the mechanical and thermal behavior of each component. A nondestructive evaluation method developed at Argonne National Laboratory uses infrared thermal imaging to provide "single-shot" full-field measurement of the distribution of thermal diffusivity in large components. By applying digital filtering, interpolation, and least-squares-estimation techniques for noise reduction, we have achieved acquisition and analysis times of minutes or less with submillimeter spatial resolution. The system has been used to examine the effects of thermal shock, oxidation treatment, density, and variations in fiber coatings in a full array of test specimens.

KEYWORDS: infrared imaging, thermal diffusivity, continuous-fiber ceramic composites, nondestructive evaluation.

---

[1]Energy Technology Division, Argonne National Laboratory, Argonne, IL.

[2]Northwestern University, Evanston IL.

[3]University of Michigan, Ann Arbor.

*Work supported by the U.S. Department of Energy, Energy Efficiency and Renewable Energy, Office of Industrial Technologies, under Contract W-31-109-ENG-38

Continuous-fiber ceramic matrix composites (CFCCs) have high strength and stability at high temperatures due to the incorporation of continuous fibers in the monolithic ceramic matrix. CFCCs are ideal replacements for traditional materials in numerous applications (including gas turbines) because of their relatively high strength and toughness at high temperatures (>1250°C) and their lower density.

Specific materials systems are desired specifically for their thermal properties, and therefore any variation in thermal diffusivity or thermal conductivity will significantly affect their ability to transfer heat properly. Such variations result from processing defects, thermal shock, or thermally induced degradation of the fiber/matrix interface and reduce the advantages for which these materials were chosen. The critical issue in most CFCC applications is therefore the distribution of thermal properties within a given component.

In this paper, we describe an infrared (IR) imaging technique for measuring thermal diffusivity of SiC/SiC CFCC specimens and components. Currently available thermal IR imaging methods are limited in that they are not portable or are very expensive.

When using IR imaging technology, the method used for thermal excitation used can be very important. Three thermal excitation methods were evaluated to determine which method is best suited for characterizing CFCC materials: (a) photothermal, (b) electrical-resistance heating, and (c) mechanical excitation. Research at Argonne has focused on photothermal excitation because it has been the most successful and allows measurement of thermal diffusivity that can be correlated to mechanical properties.

EXPERIMENTAL DETAILS

The thermal imaging system is shown in Fig. 1 and is described in an earlier paper [1]. The system utilizes Parker's method [2] to calculate thermal diffusivity, requiring a thermal pulse of short duration to be incident upon the front surface of a specimen and the temperature of the back surface to be monitored as a function of time. This was done by heating the front surface of the specimen with a photographic flash lamp and then monitoring the back surface temperature with a commercially available scanning radiometer IR camera. Images were acquired using a Mac II with an on-board frame grabber receiving standard RS-170 signals from the IR camera, digitizing each received image and then processing each image. The locally developed software extracted the average gray-scale value that represented the specimen temperature. The theoretically predicted back-surface temperature T as a function of time t and specimen thickness L according to Parker et al.[2] is given by

$$T(L,t) = \frac{Q}{\rho C L}\left[1 + 2\sum_{n=1}^{\infty}(-1)^n \exp\left(\frac{-n^2\pi^2}{L^2}\alpha t\right)\right]. \qquad (1)$$

where Q is the radiant energy incident on the front surface, ρ is density, C is specific heat, and α is thermal diffusivity. The common "half-rise time" method of determining α is to take V = 0.5 (when the back-surface temperature rise has reached half of its maximum) and ω = 1.37, thus obtaining

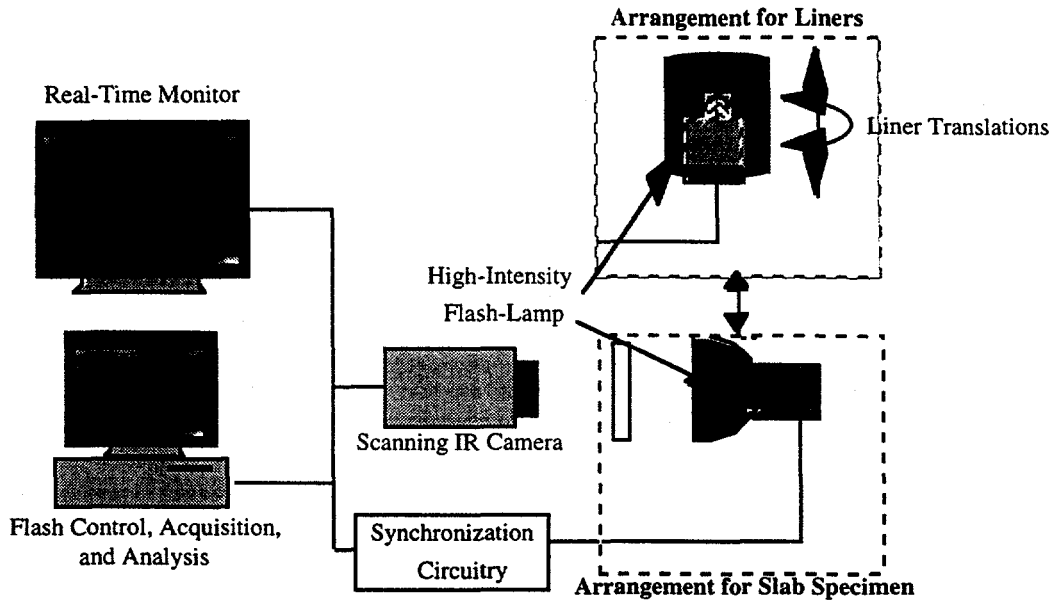

FIG. 1: Diagram of experimental arrangement used for thermal diffusivity imaging.

$$\alpha = 1.37L^2 / \pi^2 t_{\frac{1}{2}}. \qquad (2)$$

Any noise in the temperature signal significantly alters the computed thermal diffusivity value. Because of the high noise level in scanning radiometers, a noise-reduction method was considered. To minimize the time necessary to measure thermal diffusivity, a linear least-squares fit in that vicinity was used to interpolate the value of $t_{1/2}$ for the current work. By imaging the components at higher resolution than required, spatial averaging was permissible without loss of sensitivity to the minimum defect size.

For the results presented here, a 10 x 10 pixel block was used and a 512 x 413 pixel digitized image was transformed into a 51 x 41 pixel reduced image with a substantially better signal-to-noise ratio. Also, the quarter-rise time ($t_{1/4}$) and three-quarter-rise time ($t_{3/4}$) were also determined for each block, where $\omega(t_{1/4})$ = 0.92 and $\omega(t_{3/4})$ = 2.08, according to the procedure suggested in ASTM specification E 1461-92 [3].

The thermal diffusivity values obtained at these locations were averaged with that of the $t_{1/2}$ value to determine effective thermal diffusivity. This permitted determination of thermal diffusivity from a single thermal cycle, thereby reducing the total acquisition time. The resulting thermal diffusivity values for all 10 x 10 pixel subsets were assembled into diffusivity images and were stored with 16-bit resolution. This avoided the need to scale each image independently (for better comparison between images) while retaining flexibility for image enhancement in the display.

The system was further modified by incorporating a locally developed autotrigger circuit to repeatedly fire the flash, giving a dependable time for the diffusivity calculations. This autotrigger circuit has eliminated the need to manually locate the

frame of the flash, thereby providing a more precise value for the flash time.

Also used was a fully integrated, self-contained IR camera equipped with a 3-5 μm optical band-pass lens system and based on the second-generation focal plane technology. The electronics of this camera allowed for user-selectable intensity transform algorithms for contrast enhancement of the output image. Nonuniformity correction was selected to eliminate variations in pixels in the focal plane array. Automatic gain control dynamically optimized the video contrast and brightness on a frame-by-frame basis, providing additional resolution in the acquired images.

RESULTS

Calibration Specimens

Calibration samples from the National Institute of Science and Technology were used to determine the accuracy of the IR image analysis system. The absolute value of the measured thermal diffusivity using this system deviated from the calibration value by <5% due to thermal losses and approximations in the determination of $t_{1/2}$.

Thermal shock damage detection

A set of 2-D Nicalon fiber/CVI SiC composites, subjected to thermal shock testing at the University of Cincinnati [4], were studied. The set consisted of six specimens that had been shocked once at quench ΔT values of 0 (unquenched), 200, 400, 600, 800, and 1000°C, one specimen that had been quenched four times at 800°C, and a final specimen that had been air-cooled from 1000°C.

Figure 2 shows the behavior of average thermal diffusivity over the center 80% of each specimen as a function of quench ΔT, while Fig. 3 shows the behavior of the two specimens quenched at 800°C as a function of number of quench cycles. Although there is no obvious trend in either curve, each specimen shows a different diffusivity value. The variability rather than the quench history may be highly dependent on the specimens, as evidenced by the higher thermal diffusivity of the 800°C specimen quenched four times than that of the specimen quenched only once.

Al_2O_3/Al_2O_3 CFCCs

We also measured the thermal diffusivity of Al_2O_3/Al_2O_3 CFCCs. An Al_2O_3/Al_2O_3 c-ring, ≈75 mm in diameter, was sectioned into small segments ≈12 mm wide and each specimen was then examined. Because the oxide material is very translucent to the optical thermal excitation pulse, as shown in Fig. 4, it became heated volumetrically, creating a distortion from the theoretically predicted behavior in the temperature/time curve (which assumes only surface heating). Figure 5 shows temperature/time curves for the Al_2O_3/Al_2O_3 and for the same material that was painted on the flashed side to render it opaque.

The Al_2O_3/Al_2O_3 volumetric heating curve shown in Fig. 5 reached a maximum temperature much later than would be expected, based on the initial thermal response. To eliminate volumetric

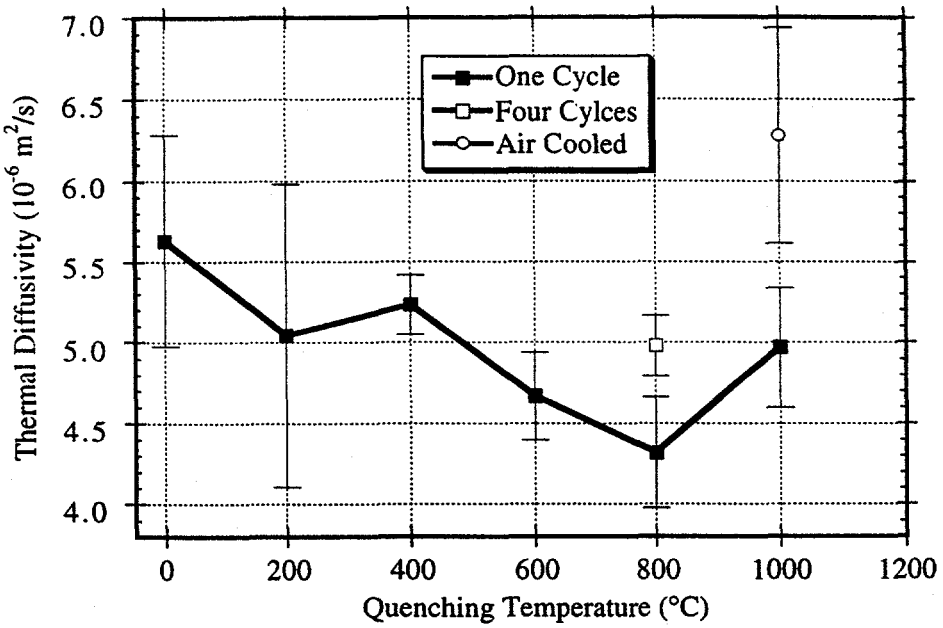

FIG. 2--Effect of quench temperature on thermal diffusivity of thermally shocked 2-D Nicalon/CVI SiC CFCC.

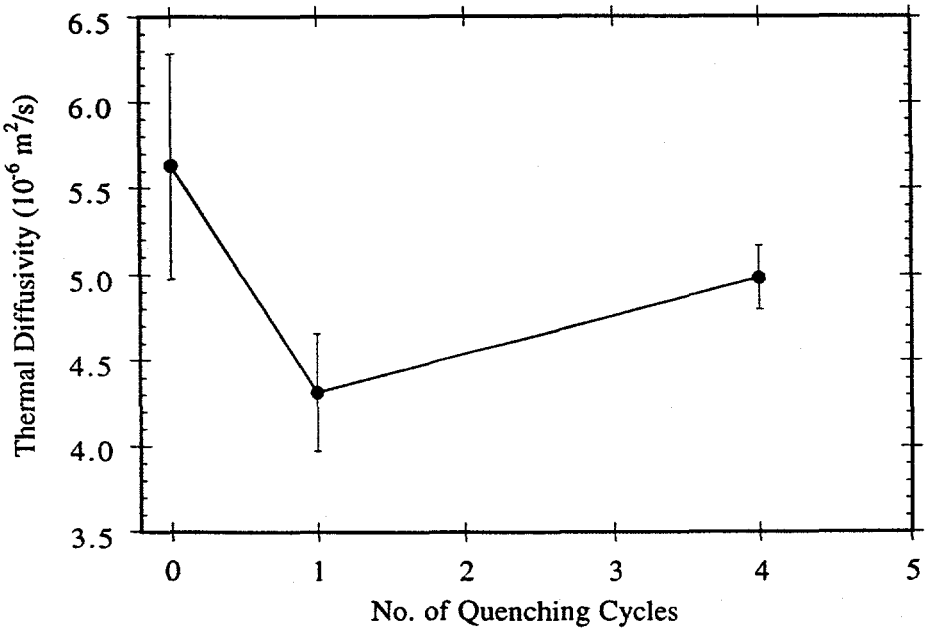

FIG. 3--Effect of number of quench cycles (@ ΔT = 800°C) on thermal diffusivity of 2-D weave Nicalon/CVI SiC CFCC.

FIG. 4--Visible image of Al_2O_3/Al_2O_3 combustor liner showing optical translucency, with interior illuminated by a glow-lamp.

heating, the specimens on the flashed side were sprayed with a graphite-based optically opaque paint. This method provided a more accurate measure of thermal variability in the specimens, and overall thermal diffusivity was seen to vary by more than a factor of 2.

The technique of coating the inside of an Al_2O_3/Al_2O_3 liner with a graphite spray was used on a test specimen made by the Babcock & Wilcox Research Center (Fig. 6). A diagram provided by Babcock & Wilcox showing the locations of the defects is given in Fig. 7. The compiled thermal diffusivity image (Fig. 8) corresponded directly to the defects shown in Fig. 7.

$SiC_{(f)}/SiC$ CFCC specimens

The system's capability was further tested to distinguish defects of various sizes in 32 "seeded-defect" $SiC_{(f)}/SiC$ composite panels made by varying several parameters such as Graphoil section thicknesses, defect sizes, fiber coatings, defect depth, and infiltration density. A diagram of one such panel, made from 12 layers of 2-D plain weave Nicalon fabric, is shown in Fig. 9. The simulated defects were created by (a) cutting out small sections of two inner plies, (b) replacing the fabric with Graphoil sections, and (c) infiltrating the weave with SiC by CVI.

Figure 10 shows images generated for one $SiC_{(f)}/SiC$ panel. Figure 10a is the raw thermal image taken at the point of maximum thermal contrast between defect and nondefect regions. Figure 10b is the same image after substantial image processing; while the defects are evident in the processed image, the relative extent of "damage" is unknown and the image processing requires expert-user interaction. Figure 10c is a thermal diffusivity image of the

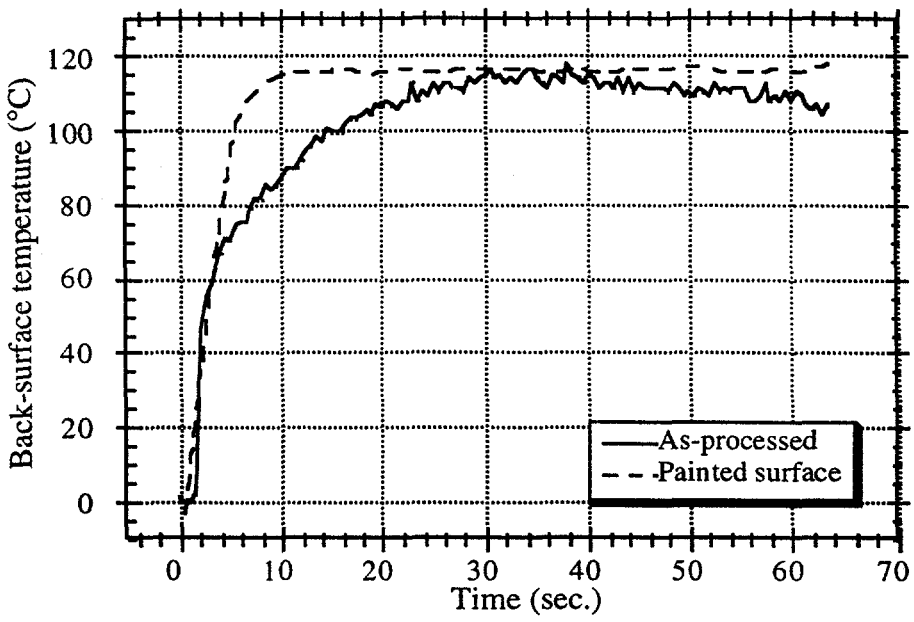

FIG. 5--Surface temperature vs. time for an Al_2O_3/Al_2O_3 CFCC in as-processed condition (volumetric heating) and with flashed surface painted to render it opaque (surface heating).

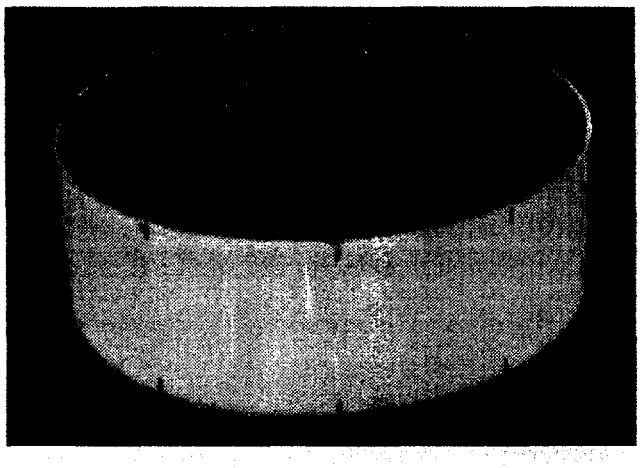

FIG. 6.--Al_2O_3/Al_2O_3 NDE standard fabricated by Babcock & Wilcox Research Center for Argonne National Laboratory. Inside of the liner was coated with graphite-based optically opaque paint.

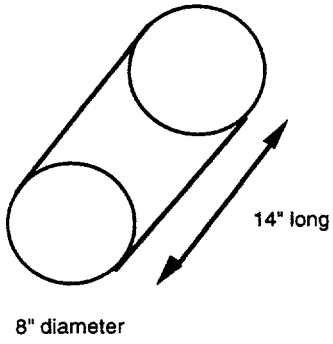

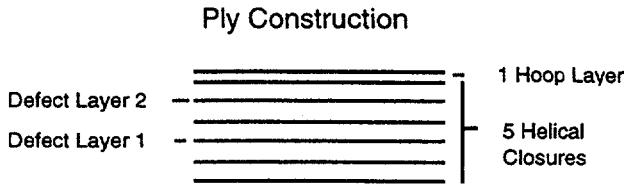

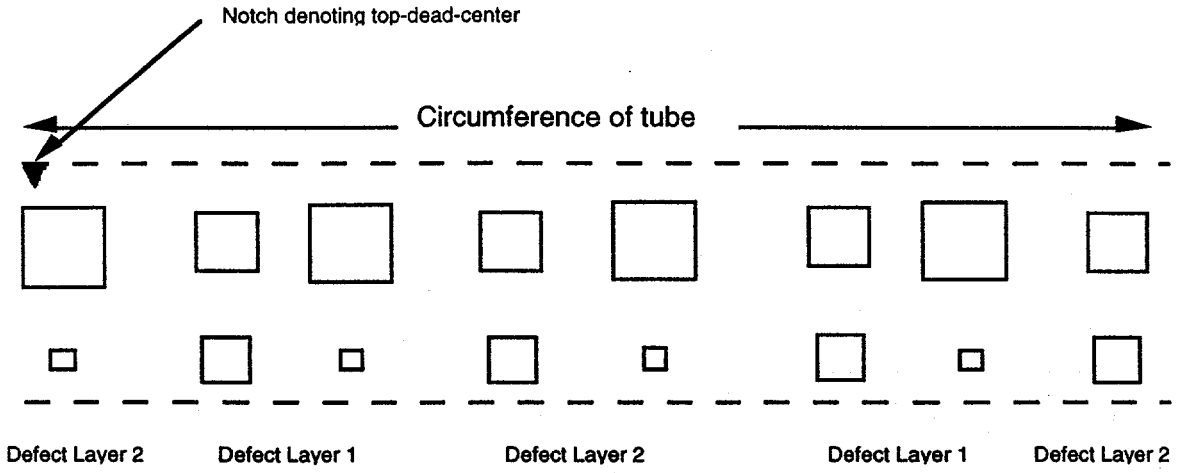

FIG. 7.--Schematic diagram of Al_2O_3/Al_2O_3 NDE standard fabricated by the Babcock & Wilcox Research Center.

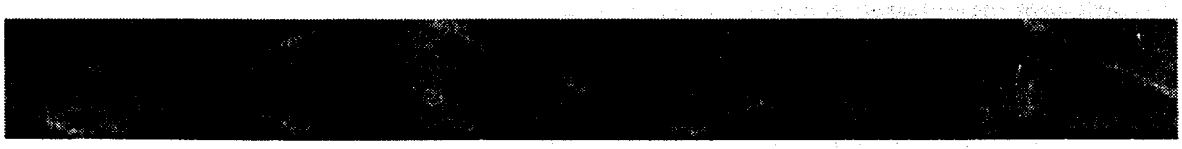

FIG. 8.--Diffusivity map of Al_2O_3/Al_2O_3 NDE standard fabricated by the Babcock & Wilcox Research Center.

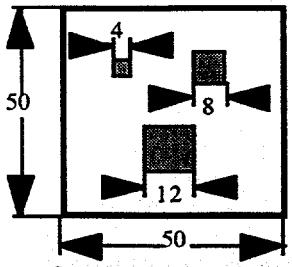

FIG. 9--Schematic diagram of seeded defect $SiC_{(f)}/SiC$ composite panels used for defect detection (dimensions in mm).

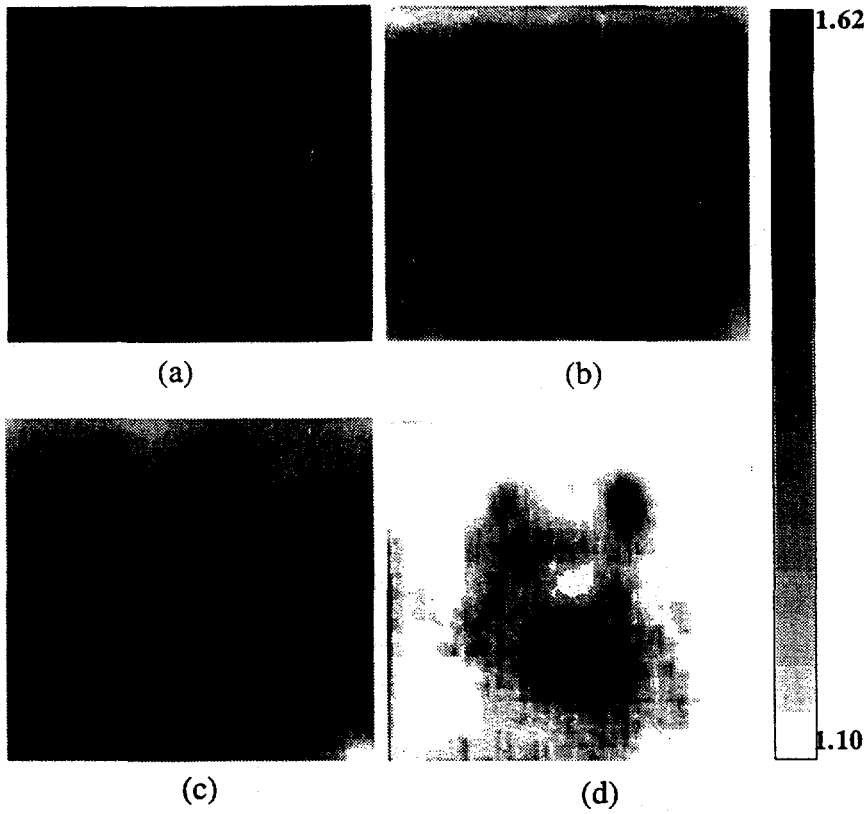

FIG. 10.--Images of $SiC_{(f)}/SiC$ composite panel. Image (a) raw thermal image, (b)processed thermal image, (c) thermal diffusivity image and (d) thermal diffusivity image with second-generation focal plane technology and user-selectable intensity transform algorithms for contrast enhancement of output image.

specimen with considerably better contrast than the processed thermal images, but with average spatial resolution. Due to the quantitative nature of the thermal diffusivity images, it is possible to directly compare defect and nondefect regions with respect to different diffusivities and porosities. Figure 10d was acquired by dynamically adjusting the gain control to optimize video contrast and brightness and provide additional resolution in the acquired image.

CONCLUSIONS

The applications of the thermal diffusivity imaging system are primarily of interest in materials characterization. During examination of actual components, the distribution of properties becomes critical, and what constitutes a potentially dangerous defect in one location might be an acceptable variation in another, less-hazardous location. We have developed a thermal diffusivity imaging method that is applicable to a wide variety of large continuous-fiber ceramic matrix composite components. Many specimens have been inspected for manufacturing-related defects. The data obtained by the thermal imaging method have been correlated to thermal shock, delaminations and density variations.

By applying digital filtering, interpolation, and least-squares-estimation techniques for noise reduction, we have achieved acquisition and analysis times of minutes or less with submillimeter spatial resolution. Images were also acquired by user-selectable intensity transform algorithms for contrast enhancement of the output image, and gain control was dynamically adjusted to optimize video contrast and brightness on a frame-by-frame basis, thus providing additional resolution in the acquired image. In the future, fatigue damage will be correlated and methods will be investigated to allow high-temperature diffusivity measurements.

REFERENCES

[1] W. A. Ellingson, S. A. Rothermel, J. F. Simpson, "Nondestructive Characterization of Ceramic Composites used as Combustor Liners in Advanced Gas Turbines", *Trans. ASME*, 95-GT-404, American Society of Mechanical Engineers, New York, NY (1995).

[2] W. J. Parker, R. J. Jenkins, C. P. Butler and G. L. Abbott, "Flash method of determining thermal diffusivity, heat capacity, and thermal conductivity," *J. Appl. Phys.*, Vol. 32 (9), pp. 1679-1684 (1961).

[3] American Society for Testing and Materials, "Standard test method for thermal diffusivity of solids by the flash method," Annual Book of ASTM Standards, ASTM E 1461-92 (1992).

[4] R. Singh and H. Wang, "Fracture and Damage: Thermal Shock Damage of CFCCs", Bi-monthly Periodical, Continuous Fiber Ceramic Composites Program, Oak Ridge National Laboratory, pp. 70-75, April-May 1994.

[5] J. S. Steckenrider, W. A. Ellingson and S. A. Rothermel, "Full-Field Characterization of Thermal Diffusivity on Continuous-Fiber Ceramic Composite Materials and Components", *Thermosense XVII: An International Conference on Thermal Sensing and Imaging Diagnostic Applications*, SPIE Proceedings Vol. 2473, S. Semanovich, Ed., Bellingham, WA, 1994.

[6] S. Ahuja, W. A. Ellingson, J. S. Steckenrider, and S. King, "Thermal Diffusivity Imaging of Continuous Fiber Ceramic Composite Materials and Components", Proceedings of the 23rd International Thermal Conductivity Conference, Nashville TN, Oct. 29-Nov. 1, 1995.

DISCLAIMER